Efficient Photomodulation of Visible Eu(III) and Invisible Yb(III) Luminescences using DTE Photochromic Ligands for Optical Encryption

Hassan Al Sabea, Lucie Norel, Olivier Galangau, Thierry Roisnel, Olivier Maury, François Riobé, Stéphane Rigaut

Article type: Full Paper

Efficient photo-modulation of visible Eu(III) and invisible Yb(III) luminescences using DTE photochromic ligands for optical encryption

Hassan Al Sabea, Lucie Norel, Olivier Galangau, Thierry Roisnel, Olivier Maury, François Riobé, and Stéphane Rigaut**

H. Al Sabea, Dr. L. Norel, Dr. O. Galangau, Prof. S. Rigaut
Univ Rennes, CNRS, ISCR (Institut des Sciences Chimiques de Rennes)-UMR 6226, F-35000 Rennes, France
E-mail: stephane.rigaut@univ-rennes1.fr, lucie.norel@univ-rennes1.fr.
Dr. O. Maury, Dr. F. Riobé,
Univ Lyon, ENS de Lyon, CNRS UMR 5182, Université Claude Bernard Lyon 1, Laboratoire de Chimie, F69342, Lyon, France

Keywords: photochromism, near infrared, luminescence, lanthanide ions, anti-counterfeiting

This work describes a complex combining three DTE units and a lanthanide ion used as an optical system displaying a double encryption method: (i) a colorful code, drawn and erased under UV and visible irradiations respectively, due to coloration and discoloration of the photochromic entities, and (ii) a concomitant gradual disappearance and progressive restoration of the associated lanthanide ion luminescence triggered with the same stimuli. The innovation of the system stems from the emission color tunability, ie. with either a lanthanide ion emitting only in the visible range (Eu^{3+}) or with another lanthanide ion emitting only in the near infrared (NIR) range (Yb^{3+}), therefore observable, or not, to the naked eye. This system is the very first one to achieve efficient repeatable modulation of pure NIR luminescence on photochemical command. Furthermore, it is proven to be highly efficient when embedded in a PDMS polymer opening real opportunities for practical applications as anti-counterfeiting.

1. Introduction

Counterfeiting is a worldwide problem that challenges companies, governments and customers.[1] Therefore, anti-counterfeiting systems that make genuine items harder to copy and easy to authenticate are important for the protection of brands, valuable documents or medicine as counterfeit substances can severely endanger human health. During the last decades, a wide variety of security technologies have been developed for advanced anti-counterfeiting and encryption (*inter alia* watermark, radio frequency identification (RFID), optical systems).[2] Nanomaterials can easily be applied inexpensively to different materials such as in security inks owing to their stimuli-induced color and/or fluorescence properties which can be detected by the naked eye,[2-5] and to further achieve physical unclonable functions (PUFs).[6-7] In that domain, typical examples are bank notes that show luminescent parts under UV light. Many markers are made of lanthanide compounds with the use of emissions and colors from lanthanide blends as security labels due to their unique spectral fingerprints[8-14] which display long lived excited state, narrow bandwidth emission band ranging from the visible to the near infra-red spectral range (NIR), and high emission efficiency. However, in a general way, conventional anti-counterfeiting and encryption based on colorimetric or fluorometric materials might be limited by spectral overlap as well as background interference, and can also be easily identified by counterfeiters and decoders. Therefore, it is imperative to develop advanced technologies that display more complicated responses.

In this context, addressable molecules have significant advantages, such as information density and complexity for more advanced encryption. This can be achieved through on/off switching of color/fluorescence in a single-mode stimulus-response. A convenient approach relies on reversible fluorescence switching with fluorophores derivatives most often associated to photochromic unit,[15-18] via intramolecular fluorescence resonance energy transfer (FRET) or electron transfer mechanism.[15,19] Such systems have been already actively incorporated into various anti-counterfeit security media for *visible* colors/luminescence switching.

Previously, some of us reported a redox-active organometallic system including an Yb^{3+} ion that can turn on/off Yb^{3+} luminescence electrochemically.[20-21] We recently added to this system an original dithienylethene (DTE) photochromic unit[16] on the β-diketonate ligands that can be efficiently switched from a non-conjugated form to a conjugated form upon UV irradiation, and switched-back using visible light to implement the very first photochemical NIR emission trigger.[22] Although this system is extremely interesting in a fundamental point of view owing to

this multifunctional stimuli association, its potential applications in devices remains limited by the long-term stability of the oxidized organometallic moiety. Note also that this system doesn't promote Eu^{3+} luminescence, probably because of quenching of the excited state by a low lying ^{3}MLCT state. On these basis, as the well-known β-diketonate complex [Eu(tta)$_3$(phen)] (tta: 2-thenoyltrifluoroacetylacetonate, phen:1,10-phenanthroline) is an efficient and stable red phosphors leading to bright red light-emitting electroluminescent devices[23-25] and as sensitization of other Ln(III) ions, including Yb^{3+}, in related complexes is highly efficient,[26-27] we decided to design the analogous compounds by simply replacing the ubiquitous tta ligand by our sophisticated photochromic DTE-β-diketone ligand with Eu^{3+} and Yb^{3+} ions (Scheme 1). Our main aim is to investigate the potential and performance of the resulting complexes for two-ways (reversible) photo-modulation of visible *and* NIR luminescence. With lanthanide ions, this photo-modulation is known in the visible range only with Eu^{3+}, and with perfectible quenching efficiency to ca. 15-30 % of the initial maximum intensity.[28-33] More generally, concerning the NIR range, only systems showing a large emission band overlapping the visible range, and thus not invisible to the naked eye, are able to promote photomodulation of their emission.[34-36]

Therefore, we report in this article a new simple system displays a potential double optical encryption method since (i) a colored form can be reversibly observed or bleached upon UV and visible irradiations, respectively, and (ii) concomitantly, vanishing of the visible (Eu^{3+}) or NIR (Yb^{3+}) lanthanide ions luminescence that can be restored. We also show that this system can be further embedded in a PDMS polymer matrix with excellent property retention: (i) colored cryptograms can be drawn and reversibly observed or erased upon UV and visible irradiations, respectively, (ii) control of the luminescence of the polymer can be concomitantly observed with quenching efficiency down to 2% of the initial maximum intensity, and (iii) excellent reversibility is observed upon multiple cycling. This system is very original since these features can be efficiently achieved with pure NIR emission totally invisible to the naked eye, potentially useful for advanced anti-counterfeiting and encryption: the Yb^{3+} system leads to an apparent classical colorimetric encryption method that is in reality much more sophisticated.[37] It is also the first system in which emission color can be tuned by a mere change of the lanthanide center, with a quenching that remains efficient from the visible to the NIR, and that opens the door to very attractive dynamic bar codes.[12]

2. Results and Discussion

2.1. Complex synthesis.

The synthesis of the new targets was conducted in two steps (Scheme 1). First, the bis-aqua precursors [M(**1o**)$_3$.2H$_2$O] **2ooo** (M = Eu^{3+}) and **3ooo** (M = Yb^{3+}) were prepared by complexation of the Eu^{3+} or the Yb^{3+} ion with three equivalents of DTE-β–diketone **1o** in its open form and, secondly, the final complexes **4ooo** (M = Eu^{3+}) and **5ooo** (M = Yb^{3+}) were achieved in CH_2Cl_2 with further coordination of phenanthroline. These new phenanthroline adducts were characterized with the help of NMR and IR spectroscopies (Supporting Information), and further identified in the fully closed form in the case of **5ccc** (M = Yb^{3+}) by X-ray diffraction (*vide infra*). Informative ^{1}H NMR spectra of **4ooo** and **5ooo** displaying the expected paramagnetic shifts (pseudo-contact shifts) were obtained for both complexes.[38-40] In particular, they show that the phenanthroline and diketonate methine protons, that are situated closest to the paramagnetic center, are the one experiencing the largest shifts. As well, clean ^{19}F NMR spectra with signals corresponding to CF_3 (-88.4 ppm) as well as to the DTE central (-132.8 ppm) and external CF_2 groups (-111.0 and -111.7 ppm) are observed for **5ooo**. Similar signals corresponding to CF_3 (-80.0 ppm) and DTE central (-132.3 ppm) and external CF_2 groups (-110.6 ppm) are observed for **4ooo**. It is worth noting that in these spectra, a single and well resolved set of signals appears for the three β-diketonate ligands that indicates a fast exchange between them. In addition, thermogravimetric analysis were performed for both complexes showing high T_{10D} of 303 and 286 °C for **4ooo** and **5ooo**, respectively, important for further integration in materials such as polymers (Figure S12, Supplementary Information).

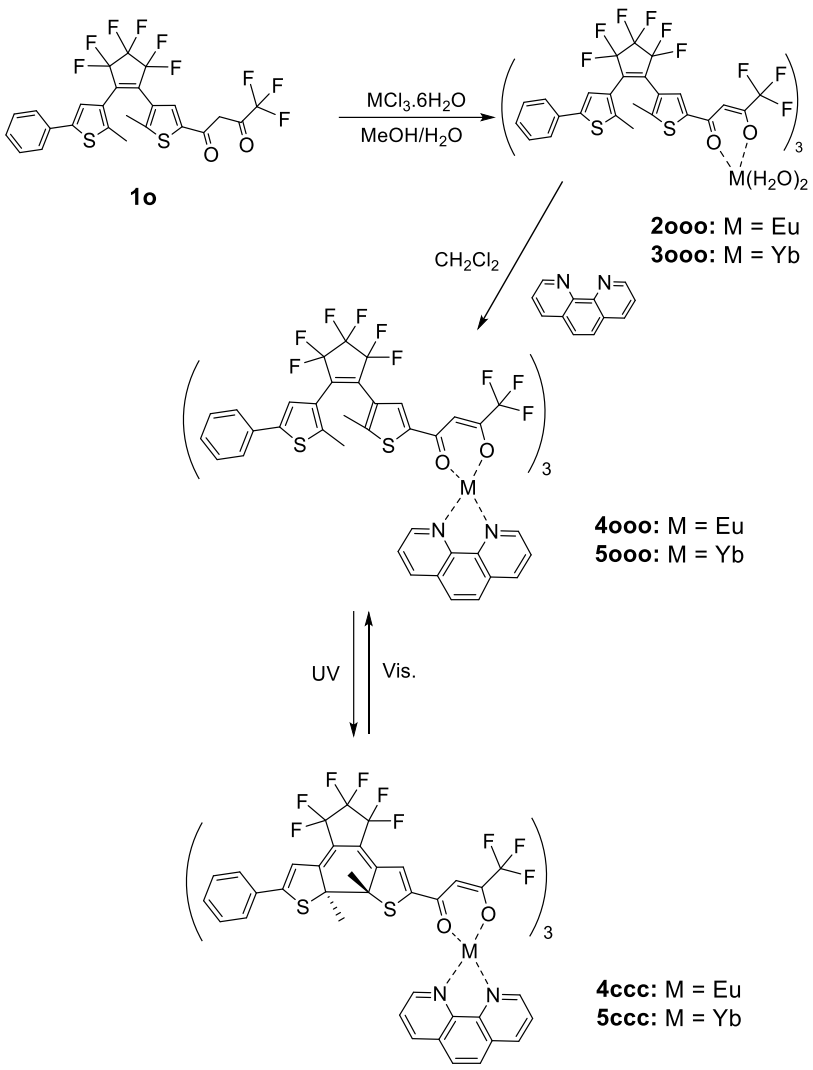

Scheme 1. Synthetic pathway yielding complexes **4ooo** and **5ooo** and their photoisomerization process to the closed analogues

2.2. Absorption spectra and photochromism of 4ooo and 5ooo.

The absorption spectra of the two complexes **4ooo** and **5ooo** in CH_2Cl_2 ([*c*] = 10^{-5} mol.L^{-1}) are identical, and a characteristic photochromism of the DTE units is observed (Figure 1 and S5, Supplementary Information). The strong absorption bands at λ_{max} = 274 and λ_{max} = 349 nm are assigned to π–π* transitions of the DTE ligand probably overlapping transitions based on the phenanthroline ligand. Upon irradiation of **4ooo** and **5ooo** solutions at λ = 350 nm to their photostationary state (PSS), a decrease of absorptions of the two bands is observed concomitantly with the rising of a broad absorption at λ_{max} = 631 nm assigned to an intra-ligand (IL) transition

centered on closed DTE moiety and a shoulder at *ca.* 390 nm (Figures 1 and S5, Supplementary Information). These solutions can be further bleached back to the pure open forms under visible light irradiation (λ = 650 nm) as attested by the quantitative recovering of the initial spectra.

Further ^{1}H NMR monitoring of the processes in CD_2Cl_2 ([*c*] ≈ 2 × 10^{-3} mol.L^{-1}) shows high photostability upon UV irradiation, ie. with (i) no detection of the NMR signals from uncoordinated phenanthroline, and (ii) well resolved signals that allow direct assessment of the PSS composition through the sequential ring-closures **ooo→ooc→occ→ccc**, thanks to the observation of four sets of signals for the phenanthroline unit protons, each being specific to one form (Supplementary information). *In fine*, integration of the α-H protons of the phenanthroline unit unambiguously shows that the photochromic conversion upon UV irradiation are almost complete with the reaching of *ca.* 92 % of overall closed isomers in the PSS for both complexes. Furthermore, the presence of only two sets of different signals for those α-H protons after irradiation and their relative integration suggest the presence of 80% of the fully closed complex **4ccc** or **5ccc** and of 20% of the one with two closed photochromic units **4occ** or **5occ**.

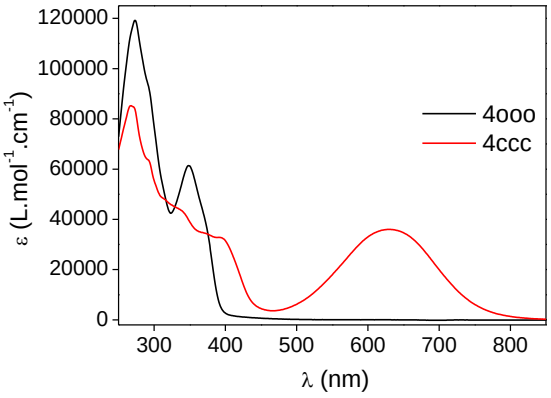

Figure 1. Absorption spectra of **4ooo** in CH_2Cl_2 solutions ([*c*]~1.4×10^{-5} mol.L^{-1}, black line) and **4ccc** (red line) obtained upon UV irradiation to PSS (λ = 350 nm). The initial spectrum was recovered after irradiation at λ = 650 nm

Good quality crystals suitable for X-ray structure determination were obtained from slow evaporation of a CH_2Cl_2 solution containing **5ccc**. A labeled view of the structure, with selected bond lengths are reported in Figure 2. The complex crystallizes in the *P-1* space group and

indirectly confirms the successful synthesis of complex **5ooo**. The bond lengths and angles are consistent with previously published complexes as [Yb(phen)(pfnp)$_3$] (Hpfnp = 4,4,5,5,5-pentafluoro-1-(2-naphthyl)-1,3-butanedione) with the Yb^{3+} ion in a slightly distorted square antiprismatic coordination polyhedron that warrants no further comments.[27] It is worth noting that, in the solid state and probably owing to the packing, for the three DTE units the C-C bond resulting from electrocyclization ranges from 1.500 to 1.602 Å.

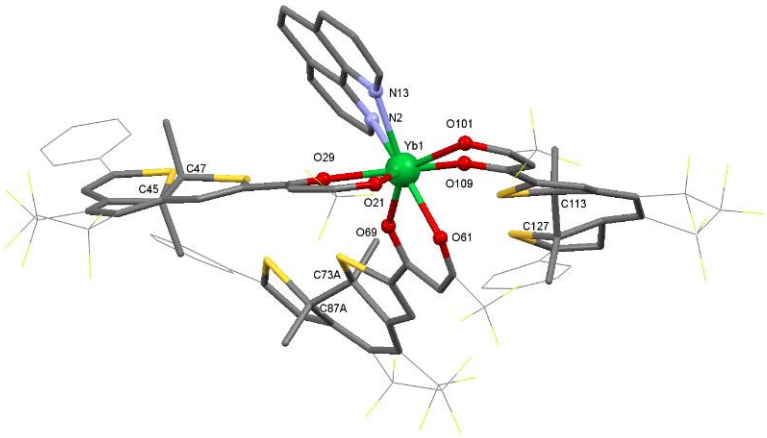

Figure 2. Simplified view of the crystal structure of **5ccc** (H atoms have been omitted). Two of the DTE units are modeled with two positions having 50% occupancy factors (see supplementary information) and only one is shown. Selected distances (Å): Yb1-N13 2.453(6), Yb1-N2 2.477(6), Yb1-O21 2.285(5), Yb1-O29 2.250(4), Yb1-O61 2.277(5), Yb1-O69 2.296(5), Yb1-O101 2.272(5), Yb1-O109 2.254(5), C87A-C73A 1.52(2), C45-C47 1.500 (13), C127-C113 1.60 (6).

2.3. Emission studies.

The emission properties of **4ooo** and **5ooo** were studied in dichloromethane solutions in aerated or degassed solutions. With a conventional fluorimeter equipped with either a NIR indium/gallium/arsenic detector or a red-sensitive photomultiplier tube, the measure of their full emission spectrum with their full intensity is difficult to achieve because of the concomitant closing of the photochromic units upon UV excitations at 350 nm providing the desired quenching pathway (*vide infra*). However, in the case of **4ooo**, under excitation with small slit aperture allowing to lower the power of excitation, and with fast scan rate, we could detect the typical features of Eu(III) ion emissions for this type of complex,[23-24] although the resolution is low (Figure 3). Therefore, we observed a sharp transition located at λ = 611 nm ($^5D_0 \rightarrow {}^7F_2$ transition) and broader bands at λ = 590 nm (J = 0), 596 nm (J = 1), 651 (J = 3) nm for others $^5D_0 \rightarrow {}^7F_J$ transitions. For the reason

discussed just above, the observed intensity of emission is then probably a bit lower than that expected, and the efficiency of the emission quenching by the closed DTE units is clearly evidenced by further loss of intensity upon measuring successively several scans. To better quantify this quenching of luminescence upon DTE isomerization, we also measured the decrease of emission at a specific wavelength (610 nm) with time upon continuous irradiation at 350 nm showing that quenching can be reached in less than a minute in these conditions. This experiment also underlines (i) the reversibility and the stability of the photomodulation (Figure 3) upon three successive closing events, and (ii) a quenching efficiency leading to a residual emission of only 1 % of the initial intensity, exceeding by far what is reported in the literature for pure optical triggering (*vide supra*).[28-33]

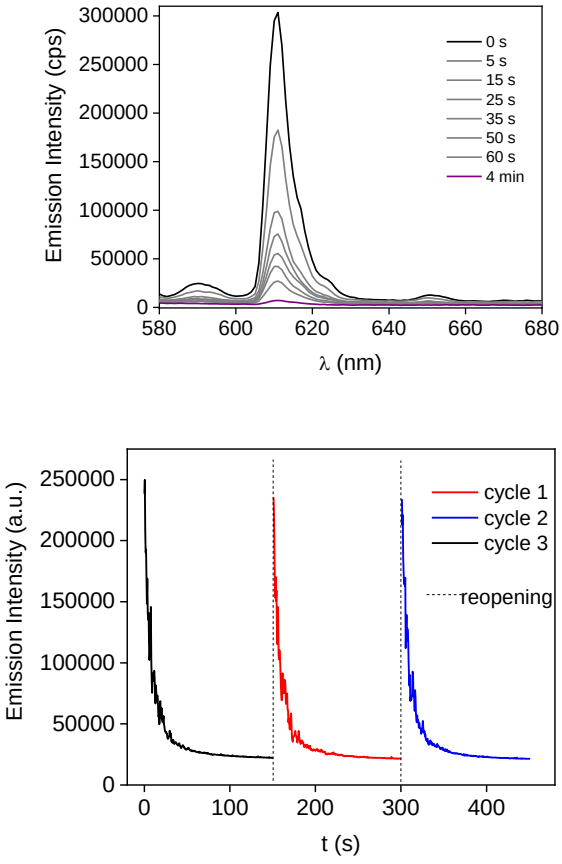

Figure 3. Emission spectra of **4ooo** (up) and emission decrease at 610 nm (down) in CH_2Cl_2 solutions ([*c*]~10^{-5} mol.L^{-1}.cm^{-1}) obtained upon continuous UV excitation at λ_{ex} = 350 nm to PSS. The initial spectra were recovered after irradiation at λ = 650 nm between each decays.

In the case of **5ooo**, although the isomerization kinetic parameters should be comparable, higher power excitation and longer integration times are required to obtain acceptable signal/noise ratio since Yb(III) emission is generally less intense than that of Eu(III).[26] However, in these conditions, closing of the DTE units is too fast and no luminescence can be detected, a fact that clearly evidences that **5ccc** is non-emissive. To obtain informative spectra on the open form, we used a N_2 cooled NIR-CCD camera detection that allows fast detection over the whole spectral range and prevent distortion of the spectrum when measuring an evolving system. Since **5ccc** is non-emissive, the obtained spectrum (Figure 4) can be assigned to **5ooo** with an emission characteristic of such diimine Yb^{3+} complex[26] with the $^2F_{5/2} \rightarrow {}^2F_{7/2}$ transition maximum detected at 970 nm (λ_{ex} = 350 nm). Also, note that whatever the type of detection used, and unlike our previously published complex associating a DTE unit with an Yb^{3+} center,[41] no emission was detected when **5ccc** was excited λ_{ex} = 650 nm to achieve sensitization with the closed form unit.

Then, luminescence quenching with DTE isomerization was followed either by the decrease of luminescence at a specific wavelength (1000 nm) upon continuous irradiation at λ_{ex} = 350 nm, or by successive acquisition of several spectra measured with CCD detection (Figure 4). Both experiments clearly demonstrate that photoisomerization leads, here again, to a very efficient quenching of Yb^{3+} based emission. In addition, to also assess the stability of the phototriggered emission response, several luminescence decreases were successively measured with regeneration of the fully open and colourless complex **5ooo** under irradiation at λ = 650 nm (Figure 4). As for the europium complex, this experiment shows (i) the high reversibility and the stability of the photomodulation upon four successive closing events with overlapping decay curves, and (ii) a quenching efficiency to leading to only 2 % of the initial intensity (Figure 4).

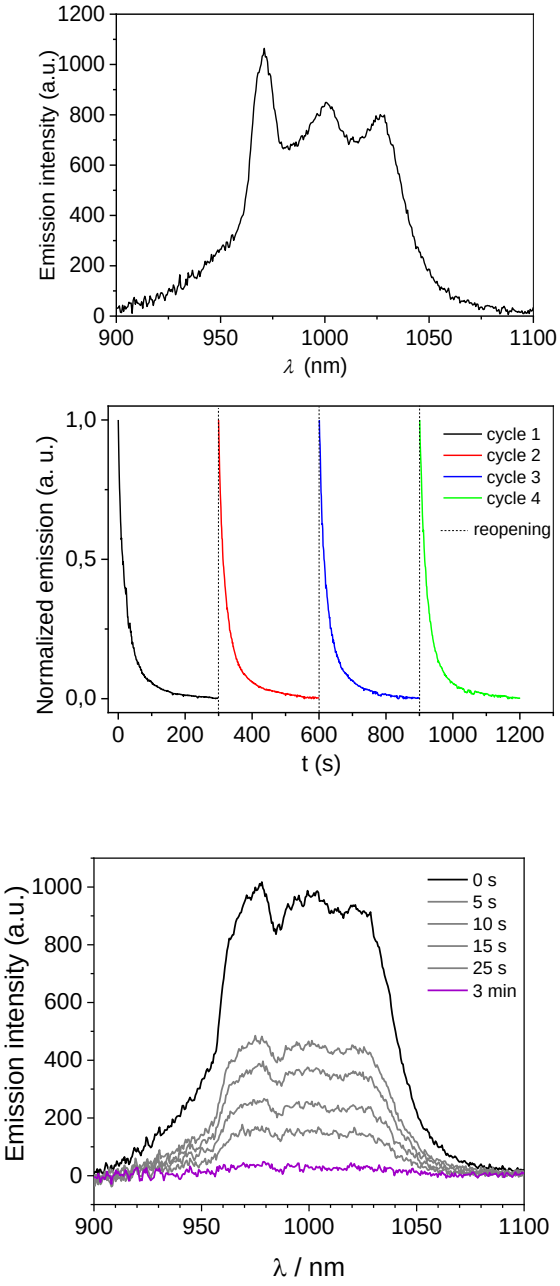

Figure 4. (up) Emission spectra of **5ooo** captured by a CCD camera (λ_{ex} = 350 nm) in CH_2Cl_2. (middle) Successive emission decrease of **5ooo** measured at 1000 nm upon UV excitation at λ_{ex} = 350 nm to PSS in CH_2Cl_2 with an indium/gallium/arsenic detector, the initial spectra were recovered after irradiation at λ = 650 nm between each decays. (bottom) Emission spectrum obtained with a NIR-CCD camera with 5 s integration time (λ_{ex} = 350 nm).

The fluorescence quenching mechanism with DTE units most often involve a non-radiative process from the excited state of the fluorophore (donor) to the photochromic unit (acceptor), generally in its conjugated state, that requires that the acceptor characteristic absorption band overlaps the emission of the donor (FRET, Förster Resonance Energy Transfer). [16] In the present case, the quenching of Eu(III) luminescence by the closed DTE-β–diketonate antenna could be easily explained by energy transfer, knowing that the closed DTE-β–diketonate low lying excited state (maximum at 631 nm or 15900 cm^{-1}, cut off at 760 nm or 13200 cm^{-1}) is lower than the best accepting $^5D_1$ and $^5D_0$ states from the europium ion ($^5D_1$ at 19 000 cm^{-1} and $^5D_0$ at 17 400 cm^{-1}).[8-11] This mechanism was previously proposed for similar Eu(III) luminescence quenching with DTE unis.[28-30] Concerning the Yb(III) ion, this overlap does not exist, the respective band maxima being distant by 340 nm (5600 cm^{-1}). The position of the $^2F_{5/2}$ excited state of Yb(III) (10200 cm^{-1}) lying at much lower energy than that of Eu(III), the quenching mechanism may proceed directly from the DTE-β–diketonate ligand triplet state probably lying bellow the $^2F_{5/2}$ excited state. Indeed, triplet pathways in DTE photochromism leading to emission quenching of metal complexes that promote inter system crossing (ISC) and concomitant DTE isomerisation to the closed form in the triplet state are well known.[42-45] However, further photophysical studies, out of the scope of this paper, will be necessary on these systems to definitely clear this point.

2.4. Polymer film fabrication and studies.

The excellent properties of these complexes make them ideal candidates for the achievement of high quality switchable luminescent materials. Therefore, the two lanthanide complexes in their open forms where incorporated in polymethylsiloxane (PDMS) polymers, a cheap and commonly used polymer for material applications. Photographs on Figure 5 show the transparency of the initial PDMS films loaded with 0.2% of **4ooo** and coloration upon closing to PSS (λ = 350 nm). The same coloration was obtained with **5ooo** in the same conditions. More precisely, the absorption spectra of both films reveal that the properties of the complexes observed in solutions were retained in the doped films for the open and the closed forms, ie. with λ_{max} = 346 nm for open forms and a slightly shifted visible absorption to λ_{max} = 611 nm (compared to λ_{max} = 631 nm in solution) for the closed forms, respectively. Several opening/closing cycles were performed (up to 27) with absorption monitoring at λ = 348 nm and λ = 615 nm that underline the stability of the complexes in the polymer film upon successive isomerization processes.

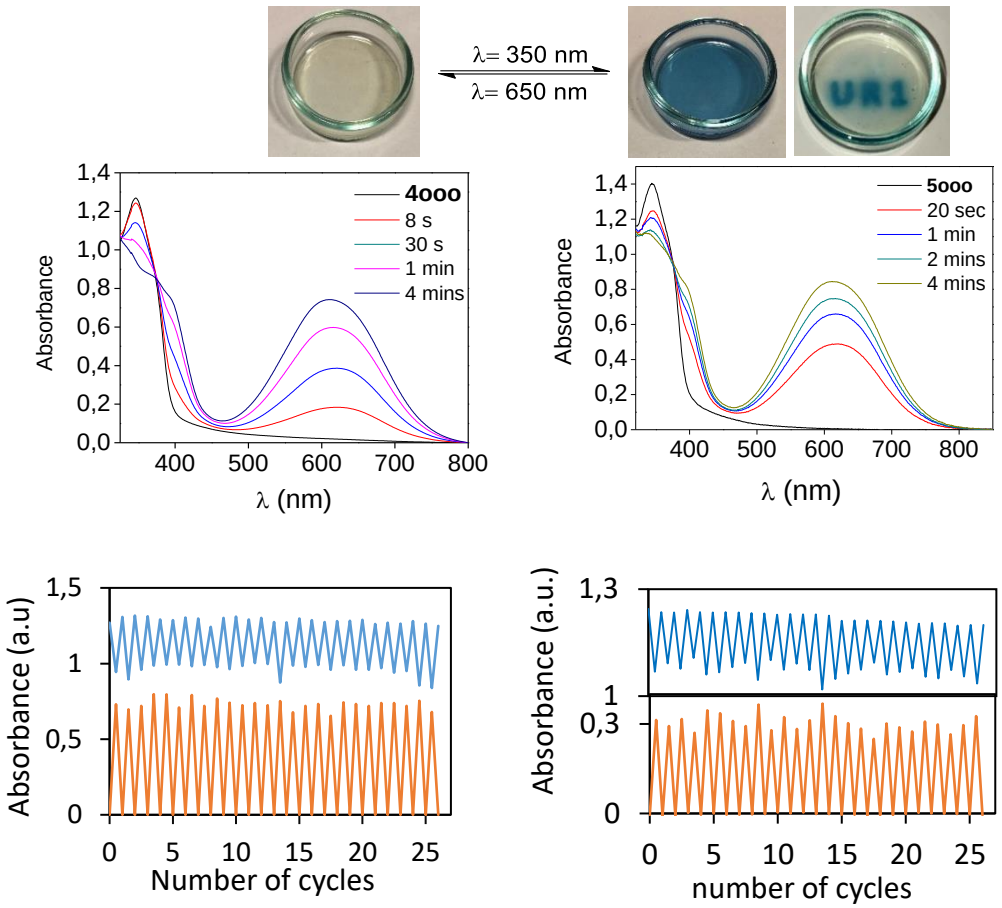

Figure 5. (up) Photographs showing the transparency of the initial films of **4ooo** and coloration upon closing to PSS (λ = 350 nm). (middle) Absorption spectrum evolutions of **4ooo** (left) and **5ooo** (right) in PDMS polymer (0.2% wt.) upon UV light irradiation to PSS (λ = 350 nm). (down) Fatigability tests performed over 27 cycles (ie. λ = 350 nm for 4 min and λ = 650 nm for 2 min) by monitoring absorption in the UV (blue line, λ= 345 nm) and in visible bands (red line, λ= 624 nm).

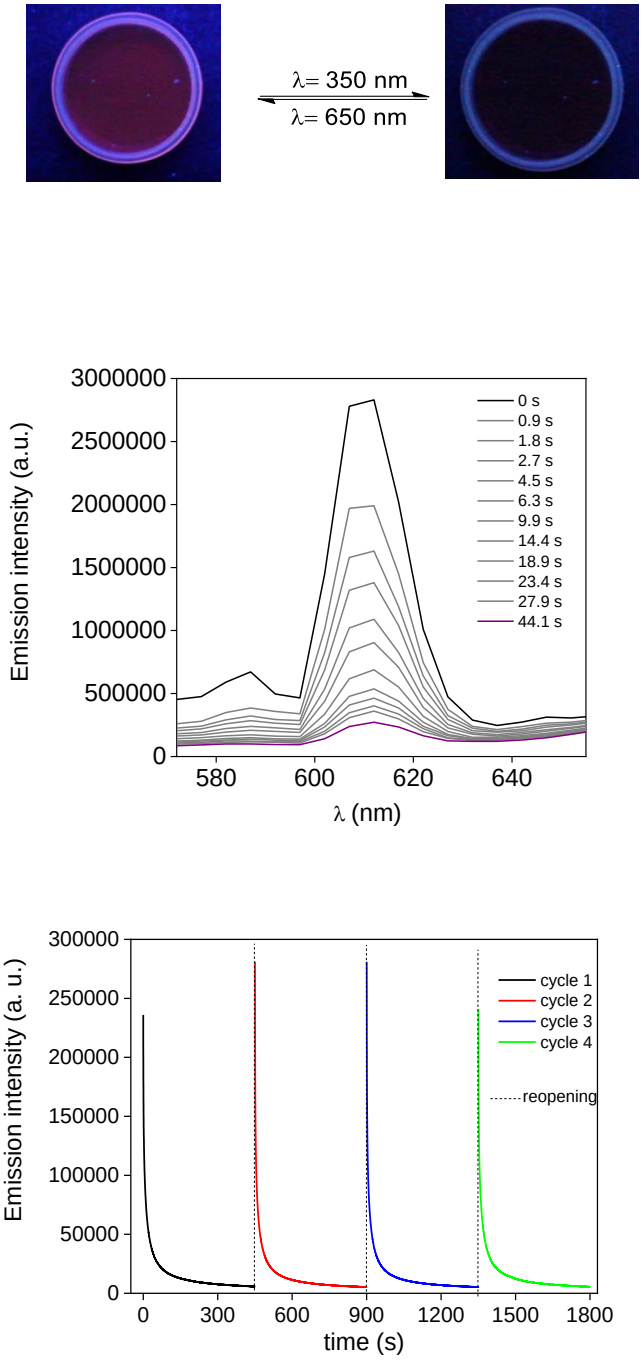

Figure 6. (up) Fluorescence photographs of **4ooo** in PDMS films (0.2% wt.) in the initial (left) and closed (PSS) (right) forms obtained by a camera through UV light excitation. (middle) Emission decrease obtained with λ_{ex} = 350 and fast scan rate (and low resolution) to observe maximum intensity (bottom) Specific decay at 1000 nm with 4 cycles (reopening was conducted with a halogen lamp with a 455 nm long pass filter for 3 min).

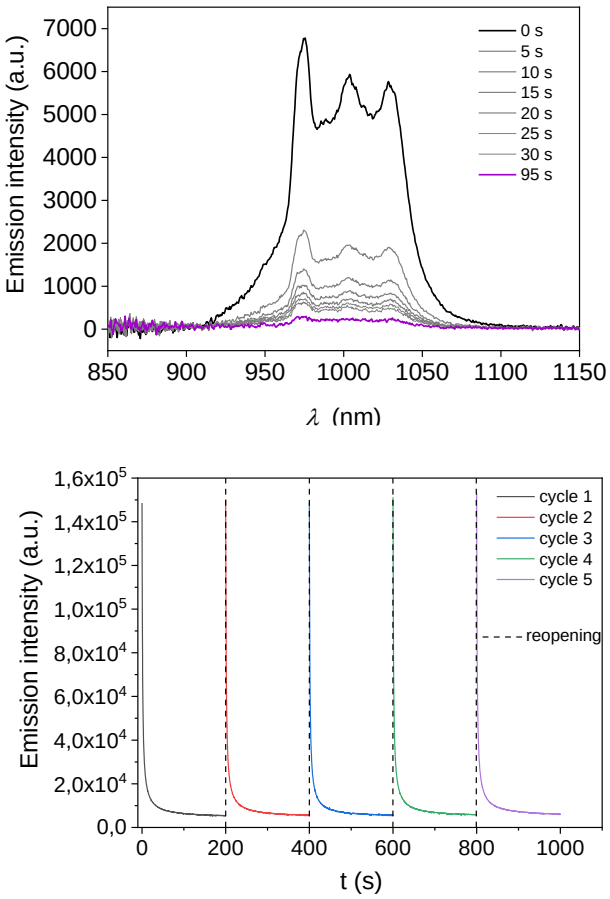

Figure 7. Emission decrease (up) of **5ooo** in PDMS films (0.2% wt.) obtained with a CCD camera with 5 s integration time (λ_{ex} = 350 nm), (down) measured at 1000 nm with a CCD camera with 0.2 s integration time upon UV excitation at λ_{ex} = 378 nm (isobestic point). Total reopening was conducted with a halogen lamp with a 455 nm long pass filter for 3 min.

Further studies of the emission properties were performed on these Eu^{3+} (Figure 6) and Yb^{3+} (Figure 7) doped polymers. The emission spectra were similar to those obtained in solution. For **4ooo**, we could observe the sharp transition located at 617 nm ($^5D_0 \rightarrow {}^7F_2$ transition), and the photomodulation of the luminescence was fully operative with a quenching to 5 % of its initial intensity after ca. 1 minute, upon UV irradiation of the film. In the case of **5ooo**, the typical Yb^{3+} emission observed in solution was also recovered in films at λ = 975 nm and a quenching to 3 % of its initial intensity was measured also after ca. 1 minute. Also, for both films, several closing/opening cycles were performed to show (i) the high stability and reversibility of the systems on an emission point of view (Figures 6 and 7), and (ii) that in the present loading and irradiation conditions, 75% quenching is obtained in 15 seconds (Eu^{3+}) or 4 seconds only (Yb^{3+}). As the reversible quenching of luminescence was perfectly visible to the naked eyes in

the case of europium, two short videos are available in the supplementary information to illustrate the color and visible emission evolutions under UV irradiation with Eu^{3+}. Note that it should be also possible to adjust the loading of the lanthanide complexes in the polymer in order to allow the desired level of detection of the two concomitant processes (blue coloration and loss of emission) together with the desired response time, depending on the expectation for applications and knowing that they are also highly dependent on the irradiation power and on the detector sensitivities.

3. Conclusion.

In this article, we reported an innovative and stable system combining three DTE units and a lanthanide ion that provides an efficient lanthanide luminescence quenching process under UV light with very high efficiency (up to 96%) that can be reversed under visible light irradiation in a highly repeatable way. In addition to the unprecedented excellent quenching efficiency for Ln ions, the novelty of the system holds in the fact that this process can be achieved with a lanthanide ion not only emitting in the visible range such as Eu^{3+}, but also with a lanthanide ion emitting in the pure near infrared (NIR) range (Yb^{3+}), therefore leading to observable emission, or not, to the naked eye. Importantly, the system is proven to be still highly efficient when embedded in a PDMS polymer for practical application and with low loading. To that regards efficient anti-counterfeiting system displaying a double optical encryption method could be imagined: (i) a colorful code can be drawn in blue and erased under UV and visible irradiations, respectively, observable to the naked eye as many systems due to coloration and discoloration of the photochromic entities, and (ii) at the same time, the gradual disappearance and progressive restoration of the associated lanthanide ion emission can be revealed under UV light.

In fine, with further extension to other Ln(III) ions, this design opens the door to complex dynamic systems displaying special fingerprints with mixture/associations of different ions and complexes in specific ratio that can be photochromic (with our ligand) or not (tta), allowing the production of markers with specific fingerprints and temporal response, including dynamic PUFs. Moreover, modification of the DTE unit should also allow color tuning giving a high potential to this system

Supporting Information
Supporting Information is available from the Wiley Online Library or from the author.

Acknowledgements
This work was supported by the Université de Rennes 1, Ecole Normale Supérieure de Lyon and the CNRS.

Received: ((will be filled in by the editorial staff))
Revised: ((will be filled in by the editorial staff))
Published online: ((will be filled in by the editorial staff))

References

[1] OECD, The Economic Impact of Counterfeiting and Piracy. OECD Publishing: Paris, 2008
[2] B. Yoon, J. Lee, I. S. Park, S. Jeon, J. Lee, J.-M. Kim, *J. Mater. Chem. C* **2013**, 1.
[3] P. Kumar, S. Singh, B. K. Gupta, *Nanoscale* **2016**, 8, 14297.
[4] X. Hou, C. Ke, C. J. Bruns, P. R. McGonigal, R. B. Pettman, J. F. Stoddart, *Nat. Commun.* **2015**, 6, 6884.
[5] W. K. Tsai, Y. S. Lai, P. J. Tseng, C. H. Liao, Y. H. Chan, *ACS Appl. Mater. Interfaces* **2017**, 9, 30918.
[6] Y. Liu, F. Han, F. Li, Y. Zhao, M. Chen, Z. Xu, X. Zheng, H. Hu, J. Yao, T. Guo, W. Lin, Y. Zheng, B. You, P. Liu, Y. Li, L. Qian, *Nat. Commun.* **2019**, 10, 2409.
[7] R. Arppe-Tabbara, M. Tabbara, T. J. Sorensen, *ACS Appl. Mater. Interfaces* **2019**, 11, 6475.
[8] A. D'Aleo, F. Pointillart, L. Ouahab, C. Andraud, O. Maury, *Coord. Chem. Rev.* **2012**, 256, 1604.
[9] E. G. Moore, A. P. S. Samuel, K. N. Raymond, *Acc. Chem. Res.* **2009**, 42, 542.
[10] S. V. Eliseeva, J.-C. G. Buenzli, *Chem. Soc. Rev.* **2010**, 39, 189.
[11] L. Armelao, S. Quici, F. Barigelletti, G. Accorsi, G. Bottaro, M. Cavazzini, E. Tondello, *Coord. Chem. Rev.* **2010**, 254, 487.
[12] O. Guillou, C. Daiguebonne, G. Calvez, K. Bernot, *Acc. Chem. Res.* **2016**, 49, 844.
[13] J. Wang, Y. Suffren, C. Daiguebonne, S. Freslon, K. Bernot, G. Calvez, L. Le Polles, C. Roiland, O. Guillou, *Inorg. Chem.* **2019**, 58, 2659.
[14] J. Andres, R. D. Hersch, J.-E. Moser, A.-S. Chauvin, *Adv. Funct. Mater.* **2014**, 24, 5029.
[15] F. M. Raymo, *Phys. Chem. Chem. Phys.* **2013**, 15, 14840.
[16] M. Irie, T. Fulcaminato, K. Matsuda, S. Kobatake, *Chem. Rev.* **2014**, 114, 12174.
[17] R. Klajn, *Chem. Soc. Rev.* **2014**, 43, 148.
[18] J. Zhang, H. Tian, *Adv. Opt. Mater.* **2018**, 6, 1701278.
[19] T. Fukaminato, T. Doi, N. Tamaoki, K. Okuno, Y. Ishibashi, H. Miyasaka, M. Irie, *J. Am. Chem. Soc.* **2011**, 133, 4984.
[20] E. Di Piazza, L. Norel, K. Costuas, A. Bourdolle, O. Maury, S. Rigaut, *J. Am. Chem. Soc.* **2011**, 133, 6174.
[21] L. Norel, E. Di Piazza, M. Feng, A. Vacher, X. Y. He, T. Roisnel, O. Maury, S. Rigaut, *Organometallics* **2014**, 33, 4824.
[22] H. Al Sabea, L. Norel, O. Galangau, H. Hijazi, R. Metivier, T. Roisnel, O. Maury, C. Bucher, F. Riobe, S. Rigaut, *J. Am. Chem. Soc.* **2019**, 141, 20026.
[23] J. Kido, H. Hayase, K. Hongawa, K. Nagai, K. Okuyama, *Appl. Phys. Lett.* **1994**, 65, 2124.
[24] C. Adachi, M. A. Baldo, S. R. Forrest, *J. Appl. Phys.* **2000**, 87, 8049.

[25] K. Binnemans, *Handbook on the Physics and Chemistry of Rare Earths*, **2005**, *225*, 107–272.
[26] S. B. Meshkova, Z. M. Topilova, D. V. Bolshoy, S. V. Beltyukova, M. Tsvirko, V. Y. Venchikov, *Acta Phys. Pol., A* **1999**, 95, 983.
[27] J. Feng, J.-B. Yu, S.-Y. Song, L.-N. Sun, W.-Q. Fan, X.-M. Guo, S. Dang, H.-J. Zhang, *Dalton Trans.* **2009**, 2406.
[28] H.-B. Cheng, G.-F. Hu, Z.-H. Zhang, L. Gao, X. Gao, H.-C. Wu, *Inorg. Chem.* **2016**, 55, 7962.
[29] H.-B. Cheng, H.-Y. Zhang, Y. Liu, *J. Am. Chem. Soc.* **2013**, 135, 10190.
[30] J. F. Mei, Z. P. Lv, J. C. Lai, X. Y. Jia, C. H. Li, J. L. Zuo, X. Z. You, *Dalton Trans.* **2016**, 45, 5451.
[31] Y. Hasegawa, T. Nakagawa, T. Kawai, *Coord. Chem. Rev.* **2010**, 254, 2643.
[32] T. Nakagawa, Y. Hasegawa, T. Kawai, *Chem. Commun.* **2009**, 5630.
[33] N. Wang, J. Wang, D. Zhao, S. K. Mellerup, T. Peng, H. Wang, S. Wang, *Inorg. Chem.* **2018**, 57, 10040.
[34] S. Bonacchi, A. Cantelli, G. Battistelli, G. Guidetti, M. Calvaresi, J. Manzi, L. Gabrielli, F. Ramadori, A. Gambarin, F. Mancin, M. Montalti, *Angew. Chem. Int. Ed.* **2016**, 55, 11064.
[35] K. Jeong, S. Park, Y. D. Lee, C. K. Lim, J. Kim, B. H. Chung, I. C. Kwon, C. R. Park, S. Kim, *Adv. Mater.* **2013**, 25, 5574.
[36] H. Lim, S. Seo, S. Pascal, Q. Bellier, S. Rigaut, C. Park, H. Shin, O. Maury, C. Andraud, E. Kim, *Scientific reports* **2016**, 6, 18867.
[37] S. Rigaut, L. Norel, H. Al Sabea, O. Galangau, O. Maury, F. Riobé, **2019,** FR-patent 1911472 (15/10/2019).
[38] G. Pintacuda, M. John, X.-C. Su, G. Otting, *Acc. Chem. Res.* **2007**, 40, 206.
[39] Z. Ahmed, K. Iftikhar, *Inorg. Chim. Acta* **2010**, 363, 2606.
[40] A. Bourdolle, M. Allali, A. D'Aleo, P. L. Baldeck, K. Kamada, J. A. G. Williams, H. Le Bozec, C. Andraud, O. Maury, *Chemphyschem* **2013**, 14, 3361.
[41] X. He, L. Norel, Y. M. Hervault, R. Metivier, A. D'Aleo, O. Maury, S. Rigaut, *Inorg. Chem.* **2016**, 55, 12635.
[42] M. N. Roberts, J. K. Nagle, J. G. Finden, N. R. Branda, M. O. Wolf, *Inorg. Chem.* **2009**, 48, 19.
[43] R. T. F. Jukes, V. Adamo, F. Hartl, P. Belser, L. De Cola, *Inorg. Chem.* **2004**, 43, 2779.
[44] M. T. Indelli, S. Carli, M. Ghirotti, C. Chiorboli, M. Ravaglia, M. Garavelli, F. Scandola, *J. Am. Chem. Soc.* **2008**, 130, 7286.
[45] C.-C. Ko, W.-M. Kwok, V. W.-W. Yam, D. L. Phillips, *Chem. – Eur. J.* **2006**, 12, 5840.

The table of contents

Keyword: photochromism, near infrared, luminescence, lanthanide ions, anti-counterfeiting

H. Al Sabea, L. Norel, O. Galangau, T. Roisnel,, O. Maury, F. Riobé, S. Rigaut

Efficient photo-modulation of visible Eu(III) and invisible Yb(III) luminescence using DTE photochromic ligands for optical encryption

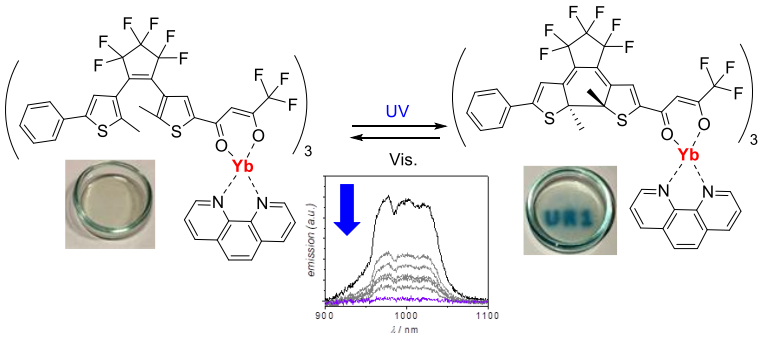

The combination of DTE-β-diketonate units with lanthanide ions allows direct reversible photocontrol visible (Eu^{3+}) and NIR (Yb^{3+}) luminescences. This system, achieving for the first time highly stable and efficient modulation of pure NIR luminescence invisible to the naked eye is proven to be still efficient when embedded in a PDMS polymer and then transferable for practical applications such as anticounterfeiting.

Supporting Information

Efficient photo-modulation of visible Eu(III) and invisible Yb(III) luminescences using DTE photochromic ligands for optical encryption

Hassan Al Sabea, Lucie Norel, Olivier Galangau, Thierry Roisnel, Olivier Maury, Francois Riobé, and Stéphane Rigaut

Table of contents

1. Synthetic procedures

General comments: Solvents were dried and distilled under argon using standard procedures. ^{1}H and ^{19}F-NMR spectra were recorded on a Bruker Avance III 400 MHz spectrometer in CD_2Cl_2 solutions at 303K. Note that for some paramagnetic lanthanide complexes, it was not possible to assign all of the signals precisely. The DTE-β–diketone **1o** and the Ytterbium bis-aqua complex **3ooo** have been obtained as previously reported.[1] $EuCl_3.6H_2O$, and 1,10-phenanthroline were purchased from Aldrich (99.998%) and used as received. Routine UV-vis irradiations were performed in UV cells or NMR tubes with a LS series Light Source of ABET technologies, Inc (150 W xenon lamp) equipped with single wavelength light filters "350FS 10-25" and "580FS 20-25". Alternatively, photoirradiations at 365 nm were performed with fluorescent tubes used for TLC illumination, and white light from a 1.5 W LED lamp (λ > 400 nm) was used for opening.

Synthetic pathway:

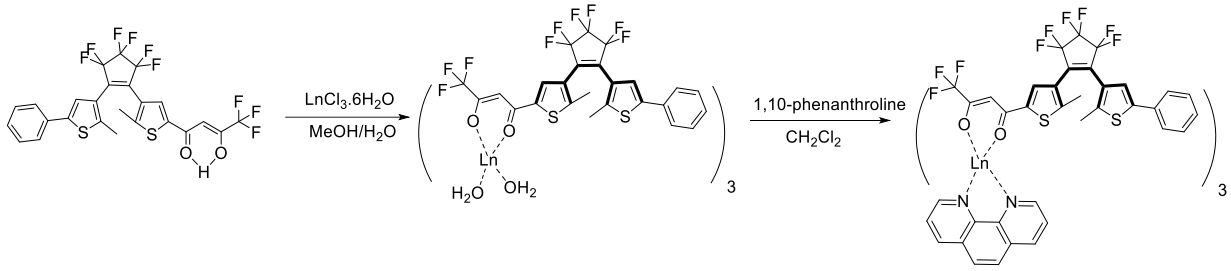

1o

Ln = Eu: **2ooo**
Ln = Yb: **3ooo**

Ln = Eu: **4ooo**
Ln = Yb: **5ooo**

Compound 2ooo: DTE compound **1o** (95 mg, 0.163 mmol) was dissolved in the minimum amount of methanol (16 mL) under ambient conditions. Then, water (3 mL) was added and the solution become cloudy, several drops of methanol were further added to obtain a clear solution. The pH of the solution was observed to be between 6 and 6.5 (otherwise the pH was maintained in this range by adding NH_4Cl in parallel). $EuCl_3.6H_2O$ (20 mg, 0.054 mmol) was dissolved in water (4 mL) and added to the solution-containing compound **1o.** A white bluish solid appeared immediately. The solution was kept stirring for 30 minutes. Excess amount of water (40 mL) was added to the solution that was further stirred for 10 minutes. The solution was filtered and washed twice with 10 mL of water and 0.5 mL of pentane. Crude compound **2ooo** was obtained as a white bluish powder dried under vacuum (100 mg, 95 % yield). ^{1}H NMR (dry CD_2Cl_2, 400MHz): δ 7.61 (d, $^{3}J_{HH}$= 8Hz, 6H, H_{meta}), 7.45 (t, 6H, $^{3}J_{HH}$= 8Hz, H_{ortho}), 7.36 (t, 3H, $^{3}J_{HH}$= 8Hz, H_{para}), 7.31 (s, 3H, H_3), 6.5 (very broad, 3H, H_1), 2.67 (bs, 9H, CH_3), 1.85 (bs, 9H, CH_3) (H_2 resonance is not detected). ^{19}F NMR (CD_2Cl_2, 376MHz): δ -81 (s, 9F, CF_3) [depending on the concentration of the sample, extreme line broadening occurs for this signal], -110.46 and -110.62 (m, 12F, CF_2), -132.25 (s, 6F, CF_2). HR-MS ESI (CH_2Cl_2): *m/z* 1896.0099 {M – $2H_2O$}$^{+}$, Calculated ($C_{75}H_{42}O_6F_{27}S_6{}^{174}Yb$) 1986.00925. Elem. Anal. Calcd for $C_{75}H_{46}F_{27}O_8S_6Yb$: H, 2.23; C, 47.5; S, 10.14 Found H, 2.65; C, 47.88; S, 9.94

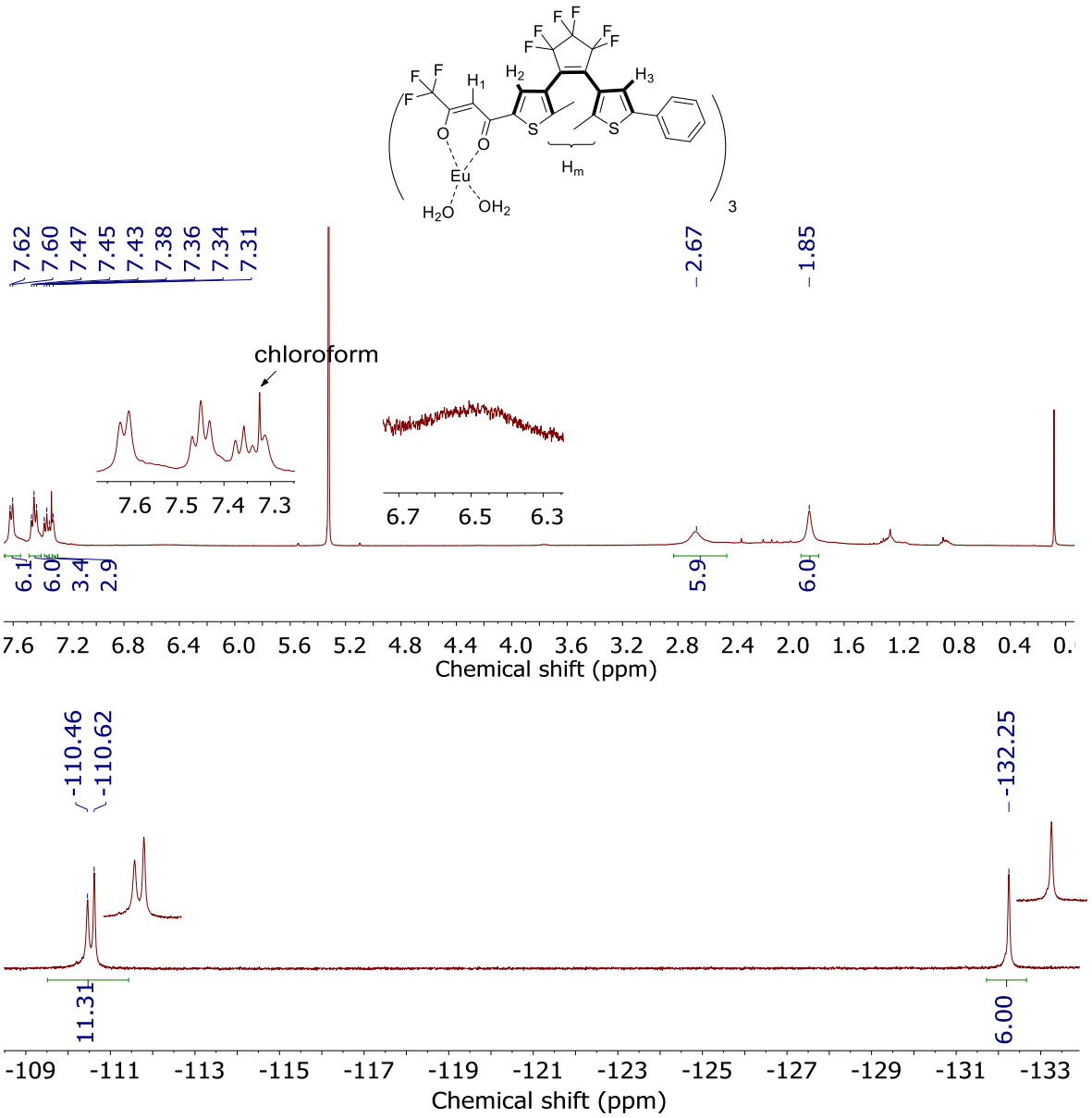

Figure S1. ^{1}H (up) and ^{19}F (down) NMR spectra of **2ooo** in CD_2Cl_2

Compound 4ooo: Compound **2ooo** (113.0 mg, 0.058 mmol) and 1,10-phenanthroline (10.6 mg, 0.058 mmol) were dissolved in 10 mL of dichloromethane and kept stirring for 24 hours under ambient conditions before evaporating the solvent under reduced pressure. Compound **4ooo** was obtained with no further purification in almost quantitative yield (115 mg, 95%). ^{1}H NMR (400 MHz, CD_2Cl_2, 297K): δ 11.13 (bs, 2H, H_{phen}), 10.02 (d, 2H, $^{3}J_{HH}$= 8Hz, H_{phen}), 9.26 (s, 2H, H_{phen}), 8.46 (d, 2H, $^{3}J_{HH}$= 8Hz, H_{phen}), 7.52 (d, 6H, $^{3}J_{HH}$= 8Hz, H_{ortho}), 7.42 (t, 6H, $^{3}J_{HH}$= 8Hz, H_{meta}), 7.34 (t, 3H, $^{3}J_{HH}$= 8Hz, H_{para}), 7.19 (s, 3H, H_2), 5.82 (s, 3H, H_3), 3.09 (s, 3H, H_1), 2.45 (s, 9H, CH_3), 1.65 (s, 9H, CH_3). ^{19}F NMR (376 MHz, CD_2Cl_2, 297 K): δ -80.05 (s, 9F, CF_3), -110.64 (t, $^{3}J_{FF}$= 7.5 Hz, 12F, 2 CF_2) *[the two external CF_2 accidentally have the same chemical shift]*, -132.31 (quintet, $^{3}J_{FF}$= 7.5 Hz, 6F, CF_2). HR-MS ESI (CH_2Cl_2): *m/z* 1675.1170 {M – **1o**+Phen}$^{+}$, Calculated (C_{74} H_{44} N_4 O_4 F_{18} S_4 ^{153}Eu) 1675.11705. Elem. Anal. Calcd for $C_{87}H_{50}F_{27}O_8S_6EuN_2$: H, 2.43; C, 50.32; S, 9.26; N, 1.35 Found H, 2.85; C, 51.10; S, 8.21; N, 1.36

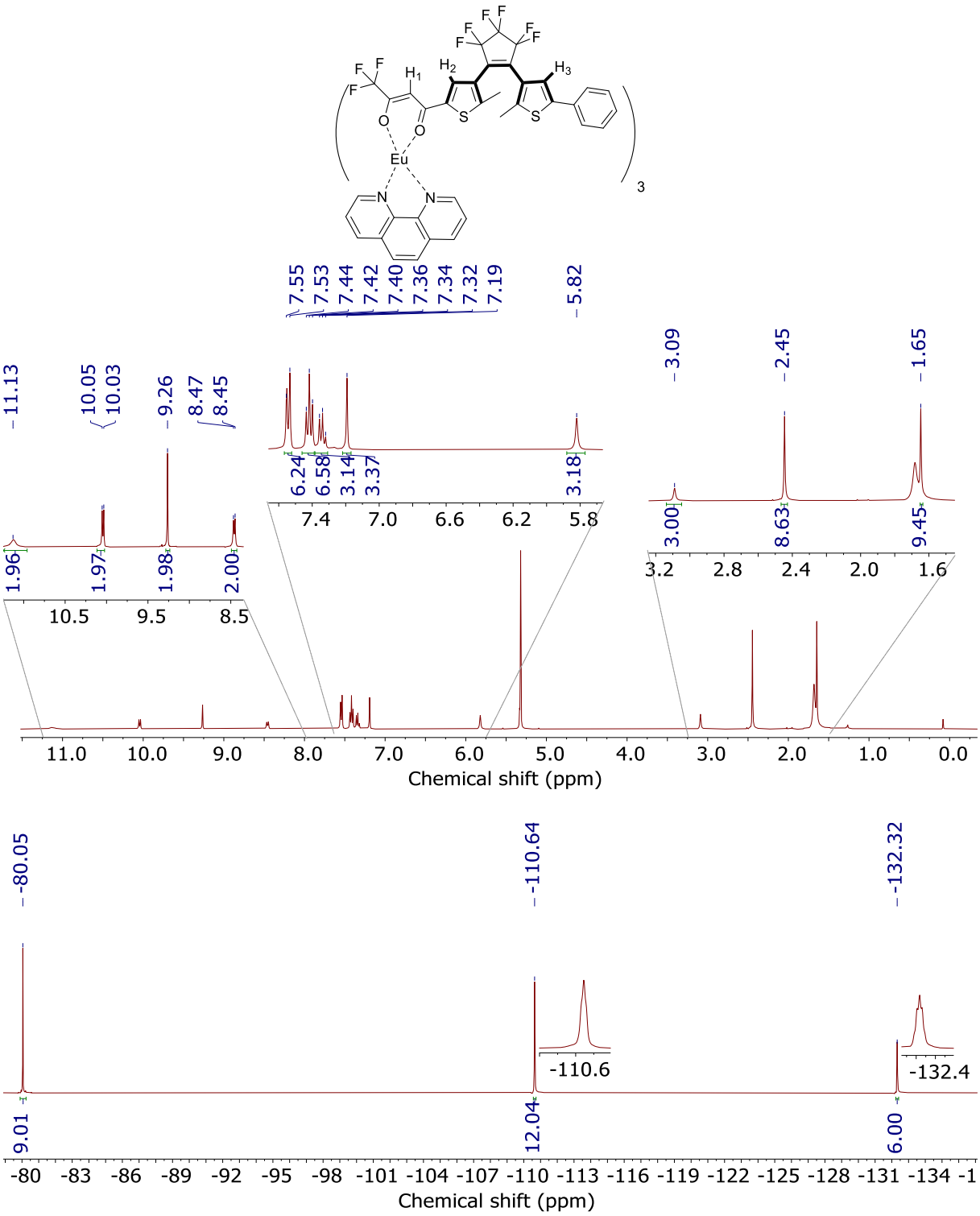

Figure S2. ^{1}H (up) and ^{19}F (down) NMR spectra of **4ooo** in CD_2Cl_2

Compound 5ooo: Compound **3ooo** (37.0 mg, 0.019 mmol) and 1,10-phenanthroline (3.4 mg, 0.019 mmol) were dissolved in 5 mL of dichloromethane in a round bottom flask and stirred for 24 hours under ambient conditions. Compound **5ooo** was obtained with no further purification in quantitative yield (40 mg, 98 % yield) after evaporating the solvent. ^{1}H NMR (400 MHz, CD_2Cl_2, 297 K): δ 18.27 (bs, 2H, H_{phen}), 17.46 (bs, 2H, H_{phen}), 12.96 (bs, 2H, H_{phen}), 10.41 (bs, 2H, H_{phen}), 7.54 (apparent doublet, 15H, H_2 and $H_{ortho/meta}$), 7.43 (m, 3H, H_{para}) *[the*

phenyl signals show a case of virtual coupling due to accidentally equal chemical shift for the meta and ortho protons], 6.85 (s, 3H, H_3), 1.36 (s, 9H, CH_3), 1.34 (s, 9H, CH_3), -10.14 (s, 3H, H_1). ^{19}F NMR (376 MHz, CD_2Cl_2, 297 K): δ -88.36 (s, 9F, CF_3), -111.03 (bs, 6F, CF_2), -111.69 (bs, 6F, CF_2), -132.83 (quintet, $^3J_{FF}$= 7.5 Hz, 6F, CF_2). HR-MS ESI (CH_2Cl_2): *m/z* 1516.060 {M – **1o**}$^+$, Calculated ($C_{62}H_{36}N_2O_4F_{18}S_4{}^{174}Yb$) 1516.06593. Elem. Anal. Calcd for $C_{87}H_{50}F_{27}O_8S_6YbN_2$: H, 2.40; C, 49.81; S, 9.17; N, 1.34 Found H, 2.76; C, 50.44; S, 8.91; N, 1.13.

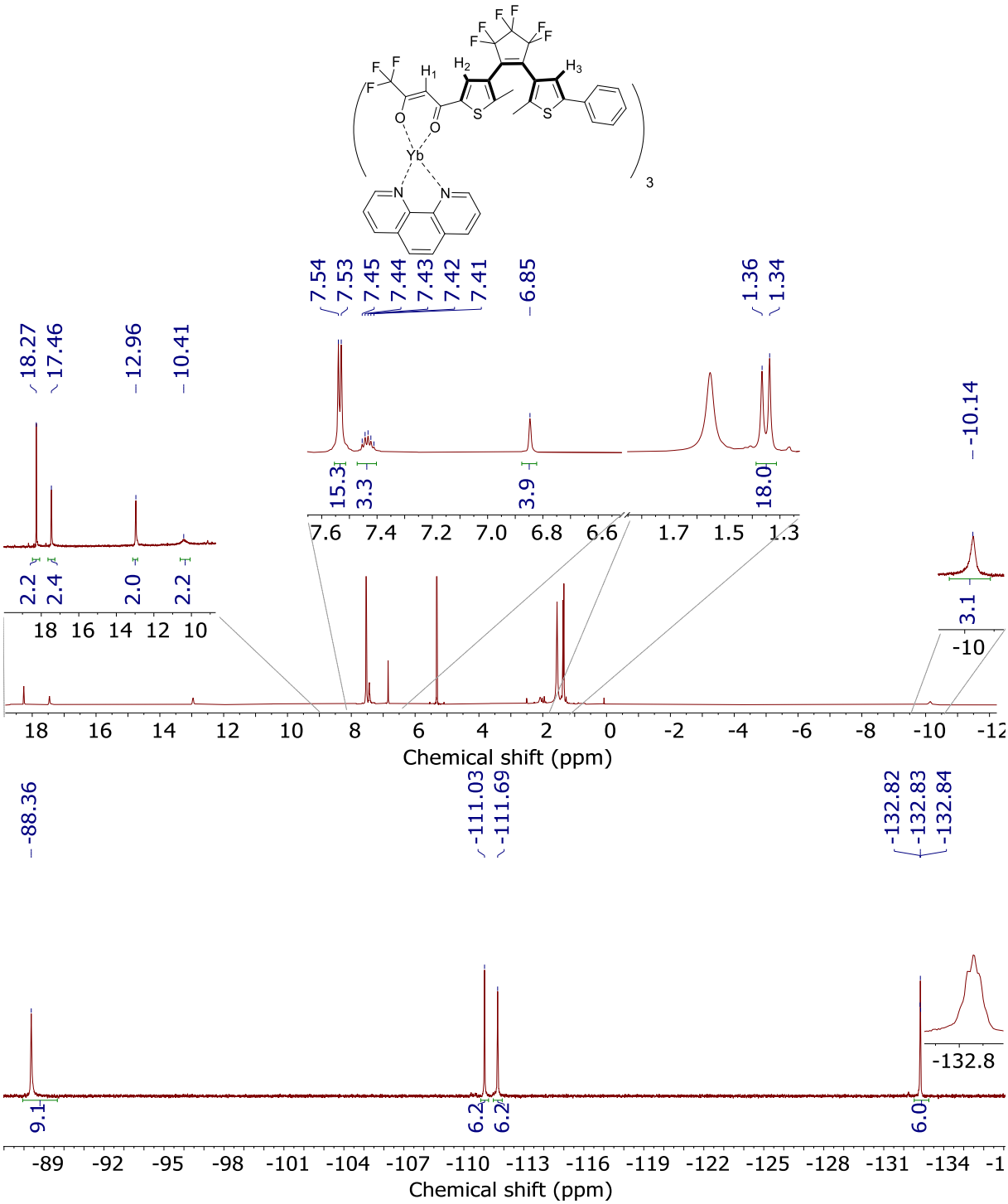

Figure S3. ^{1}H (up) and ^{19}F (down) NMR spectra of **5ooo** in CD_2Cl_2

2. Crystallographic studies

General comments: X-Ray measurements were performed at 150(2) K with a crystal mounted mounted with a cryoloop on the goniometer head of a D8 Venture Bruker AXS diffractometer (multilayer monochromator, Mo Kα radiation, λ = 0.710 73 Å). The structure was solved by dual-space algorithm using the *SHELXT* program,[2] and then refined with full-matrix least-squares methods based on F^2 (*SHELXL*).[3] The contribution of the disordered solvents to the calculated structure factors was estimated following the *BYPASS* algorithm,[4] implemented as the *SQUEEZE* option in *PLATON*.[5] A new data set, free of solvent contribution, was then used in the final refinement. All non-hydrogen atoms of the non-disordered parts of the molecule were refined with anisotropic atomic displacement parameters. H atoms were finally included in their calculated positions and treated as riding on their parent atom with constrained thermal parameters. A final refinement on F^2 with 21405 unique intensities and 1053 parameters converged at ωR_F^2 = 0.2009 (R_F = 0.0819) for 15969 observed reflections with $I > 2\sigma(I)$. CCDC 1992959 contains the supplementary crystallographic data for this paper. These data can be obtained free of charge from The Cambridge Crystallographic Data Centre via www.ccdc.cam.ac.uk/data_request/cif.]

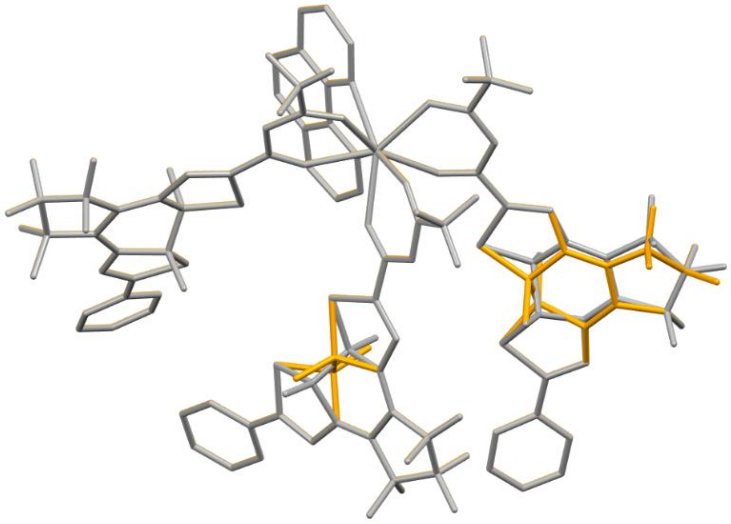

Figure S4. Simplified view of the crystal structure of **5ccc** showing the two positions (50 % occupancy factor) of two of the DTE cores.

Table S1. Crystal data and structure refinement parameters for **5ccc**.

	5ccc
Formula	$C_{87}H_{50}F_{27}N_2O_6S_6Yb$
FW	3095.65
Cryst. Syst.	triclinic
Space group	P-1
a (Å)	11.7182(18)
b (Å)	18.063(3)
c (Å)	22.900(4)
α (°)	85.553(7)
β (°)	82.054(6)
γ (°)	77.440(6)
V (Å3)	4680.07
Z	2
Dca (g.cm-3)	1.849
T (K)	150(2)
Final R (I > 2□)	0.0819
Rw (all)	0.2237

Table S2. Selected bond lengths from **5ccc**.

Bond	**Bond length**
Yb1-N13	2.453(6)
Yb1-N2	2.477(6)
Yb1-O21	2.285(5)
Yb1-O29	2.250(4)
Yb1-O61	2.277(5)
Yb1-O69	2.296(5)
Yb1-O101	2.272(5)
Yb1-O109	2.254(5)
C87A-C73A	1.52(2)
C45-C47	1.500(13)
C127-C113	1.60(6)

3. UV-Vis studies and photochromic reactions.

General comments: UV-vis measurements were performed in CH_2Cl_2 at 20 °C using a "analytikjena specord 205" spectrophotometer. UV-vis irradiations were performed in UV cells or NMR tubes with a LS series Light Source of ABET technologies, Inc (150 W xenon lamp), with single wavelength light filters "350FS 10-25" and "650FS 20-25".

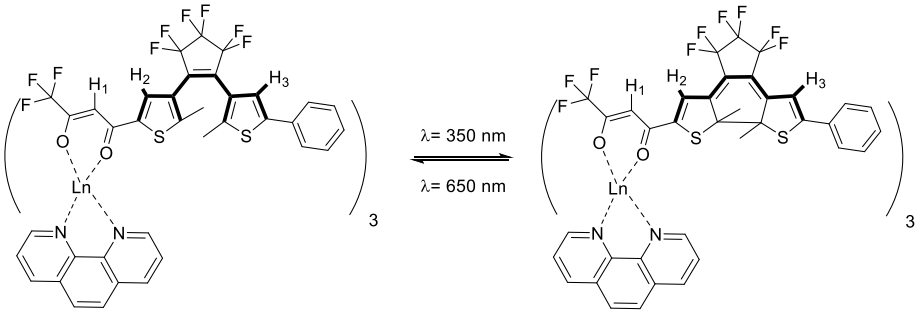

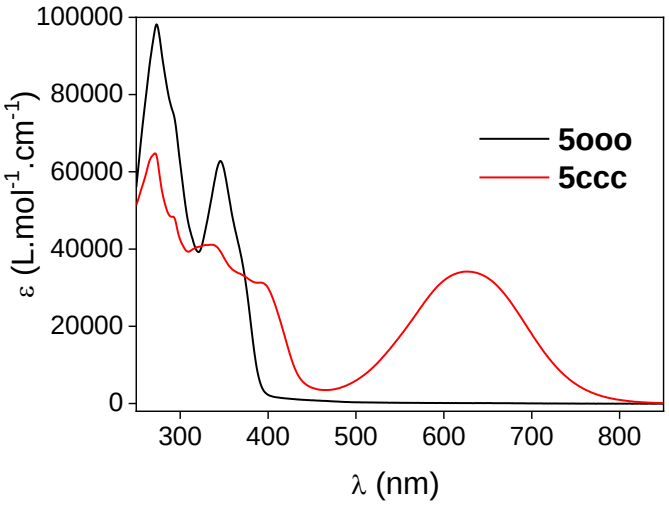

Figure S5. Absorption spectra of **5ooo** in CH_2Cl_2 solutions ([c]~1.4×10^{-5} mol.L^{-1}) and **5ccc** obtained upon UV irradiation to PSS (λ = 350 nm). The initial spectrum was recovered after irradiation at λ = 650 nm.

Study of the photo-stationary state:

For complex 5ooo:

In order the estimate the composition of the PSS, compound **5ooo** was fetched in an NMR tube ([c] ≈ 10^{-3} mol.L^{-1}) and subjected for 24 hours to UV irradiation (λ= 350 nm) under ambient conditions. Upon following ^{1}H and ^{19}F NMR spectrum upon irradiation and focusing on CF_3 and phenanthroline protons, four different species are observed, the initial fully opened compound **5ooo**, the fully closed one **5ccc**, and the two intermediates (compound **5ooc** bearing one closed DTE unit and compound **5occ** bearing two closed DTE units). After 30 minutes under 350 nm, the NMR spectrum (fade green in figure 6) shows three different species: 18% **5occ**, 41% **5ooo**, and 41% **5ooc** (integration of the α-H protons of the phenanthroline unit). After 3 hours, no more initial compound **5ooo** is seen, whereas the other

three different species are observed in the following ratio: 42% **5occ**, 42% **5ccc**, and 16% **5ooc.** After 24 hours, no more evolution takes place (PSS). Relying on the integration of these phenanthroline protons, the PSS was estimated to be composed of 80% of **5ccc** and 20% of **5occ**.

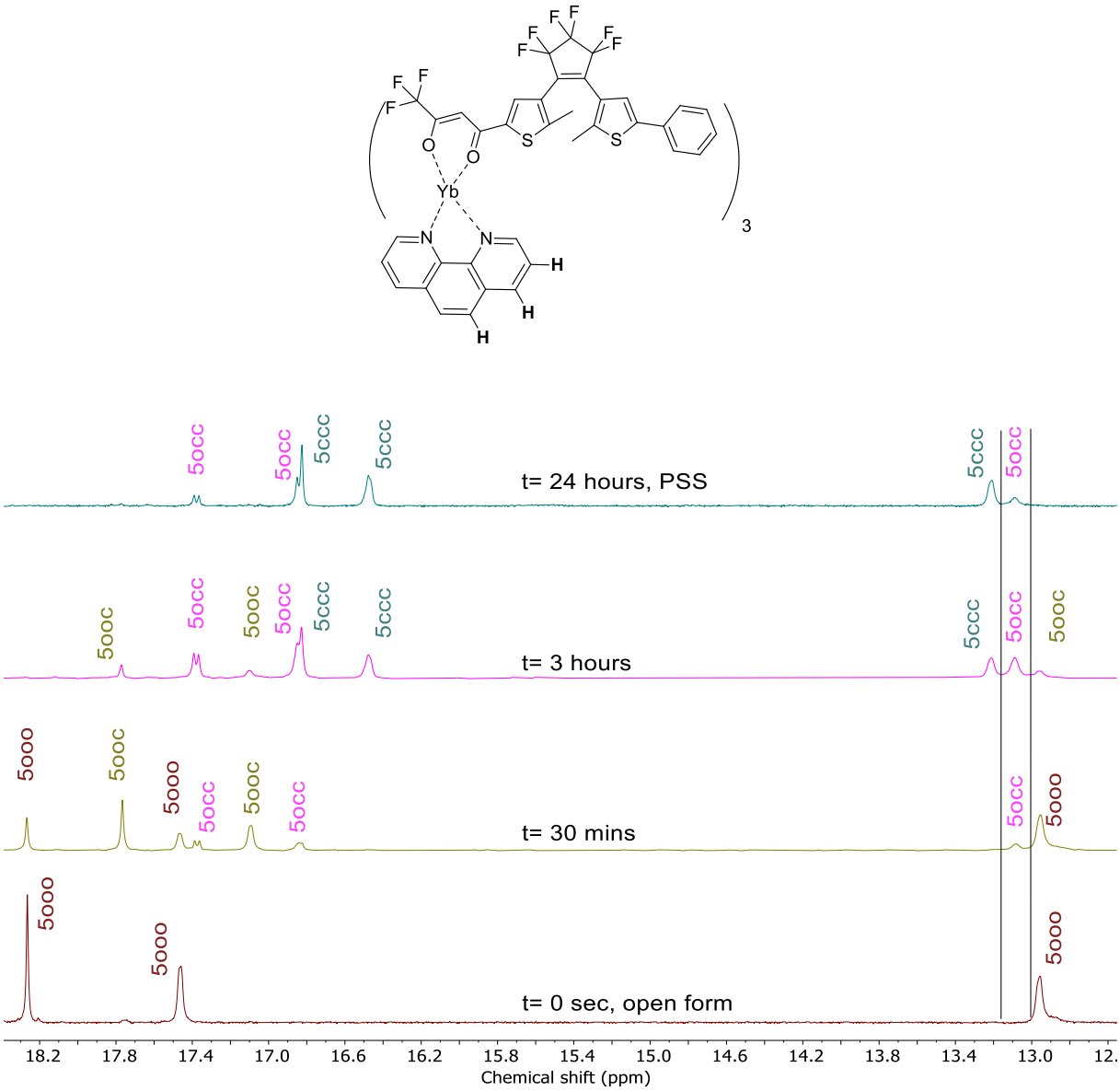

Figure S6. Evolution of selected ^{1}H NMR signals of **5ooo** in CD_2Cl_2 upon irradiation at λ= 350 nm for 24 hours. The assignment is based on the time evolution of the system. The initial spectrum was recovered after irradiation at λ = 650 nm.

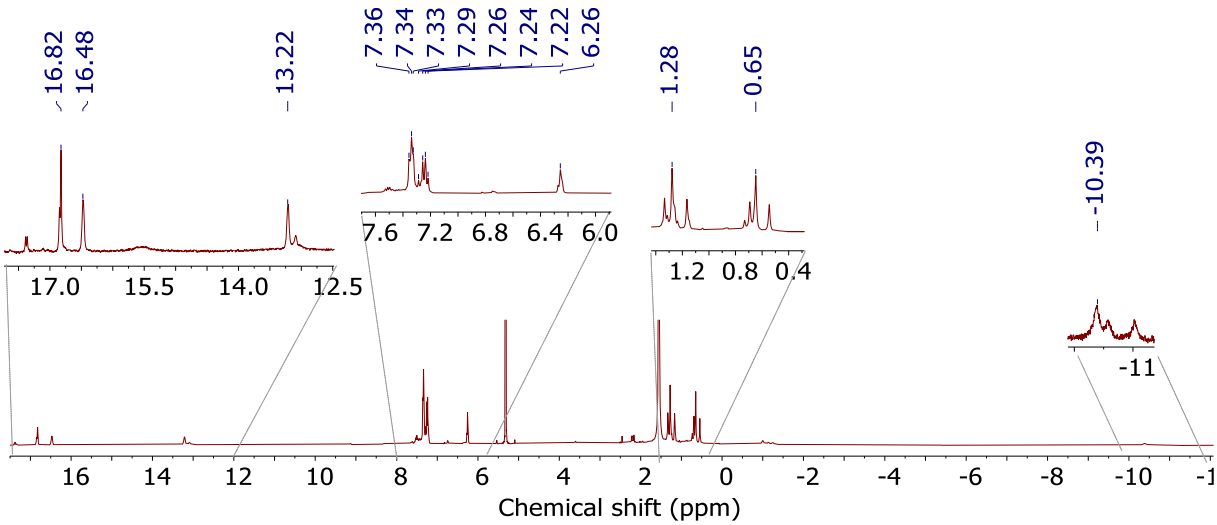

Figure S7. Full ^{1}H NMR spectrum of iradiated **5ooo** to PSS in CD_2Cl_2 (λ = 350 nm for 24 hours)

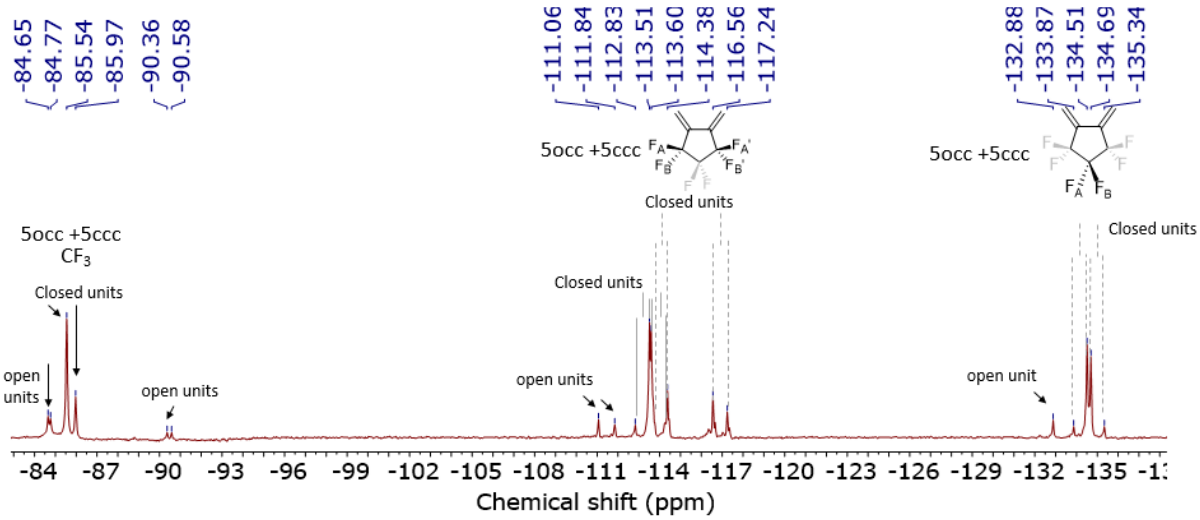

Figure S8. ^{19}F NMR full spectrum iradiated **5ooo** to PSS in CD_2Cl_2 (λ = 350 nm for 24 hours), *the pattern of the spectrum is due to the presence of statistical isomers for* ***5occ*** *(occ, coc, cco)*

Compound 5ccc: ^{1}H NMR (400 MHz, CD_2Cl_2, 297 K): δ 16.86 (bs, 2H, H_{phen}), 16.51 (bs, 2H, H_{phen}), 13.26 (bs, 2H, H_{phen}), 7.55-7.26 (m, 18H, H_{phenyl} + H_2), 6.30 (s, 3H, H_3), 1.32 (s, 9H, CH_3), 0.69 (s, 9H, CH_3), -10.35,-10.98 (s, 3H, CH_1). ^{19}F NMR (376 MHz, CD_2Cl_2, 297 K): δ -85.54 (s, 6F, CF_3), -85.97 (s, 3F, CF_3), -113.17 (d, 3F, $^{2}J_{FF}$= 250 Hz, external CF_2), -113.92 (d, 3F, $^{2}J_{FF}$= 250 Hz, external CF_2), -114.03 (d, 3F, $^{2}J_{FF}$= 253 Hz, external CF_2), -116.90 (d, 3F, $^{2}J_{FF}$= 235 Hz, external CF_2), -134.19 (d, 3F, $^{2}J_{FF}$= 235 Hz, central CF_2), -135.0 (d, 3F, $^{2}J_{FF}$= 235 Hz, central CF_2).

For complex 4ooo:

Similar experiments in the same conditions for **4ooo** led to similar results, ie. **to** 80% of **4ccc** and 20% of **4occ** at PSS.

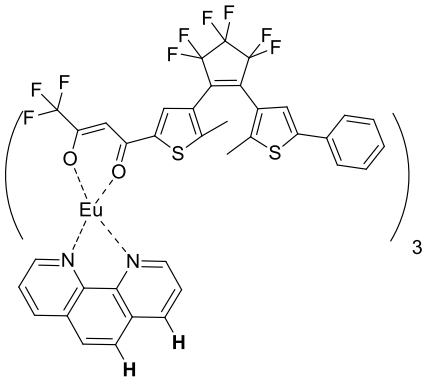

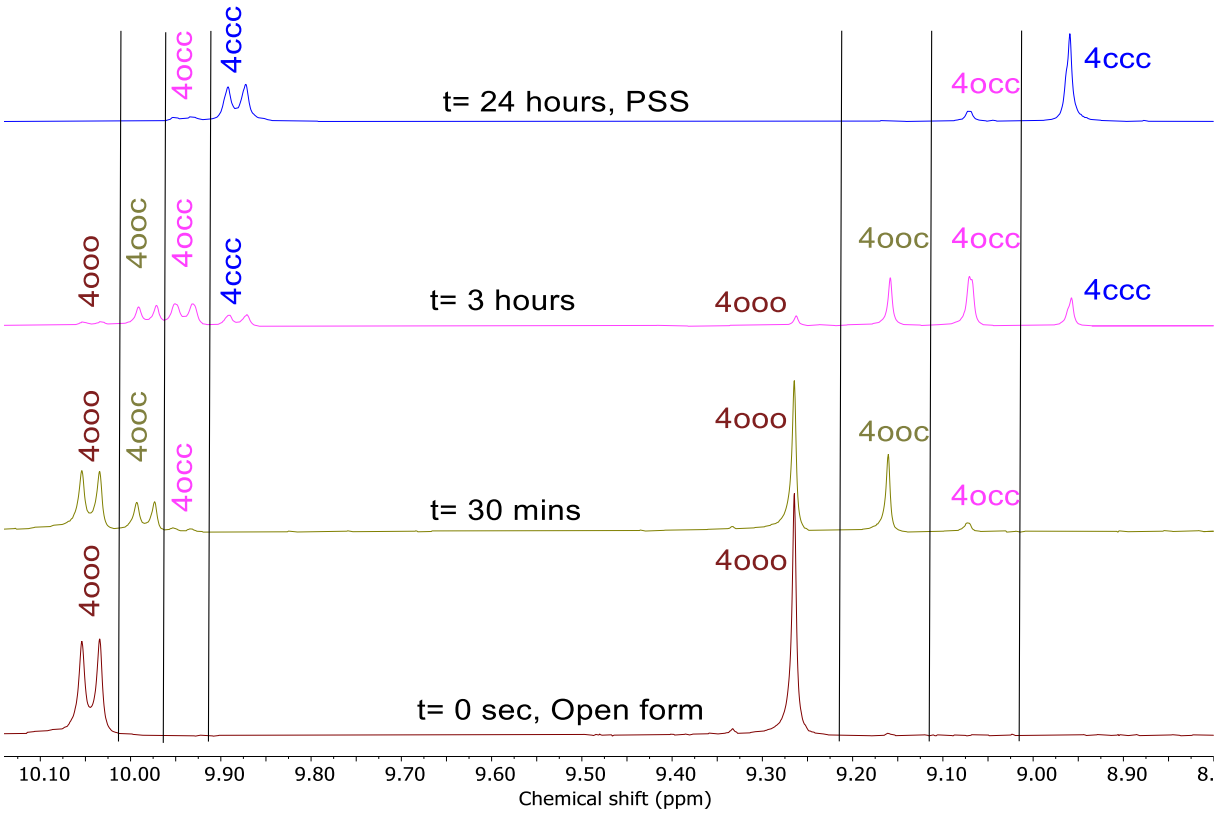

Figure S9. Evolution of selected ^{1}H NMR signals of **4ooo** in CD_2Cl_2 upon irradiation at λ= 350 nm for 24 hours. The assignment is based on the time evolution of the system. The initial spectrum was recovered after irradiation at λ = 650 nm.

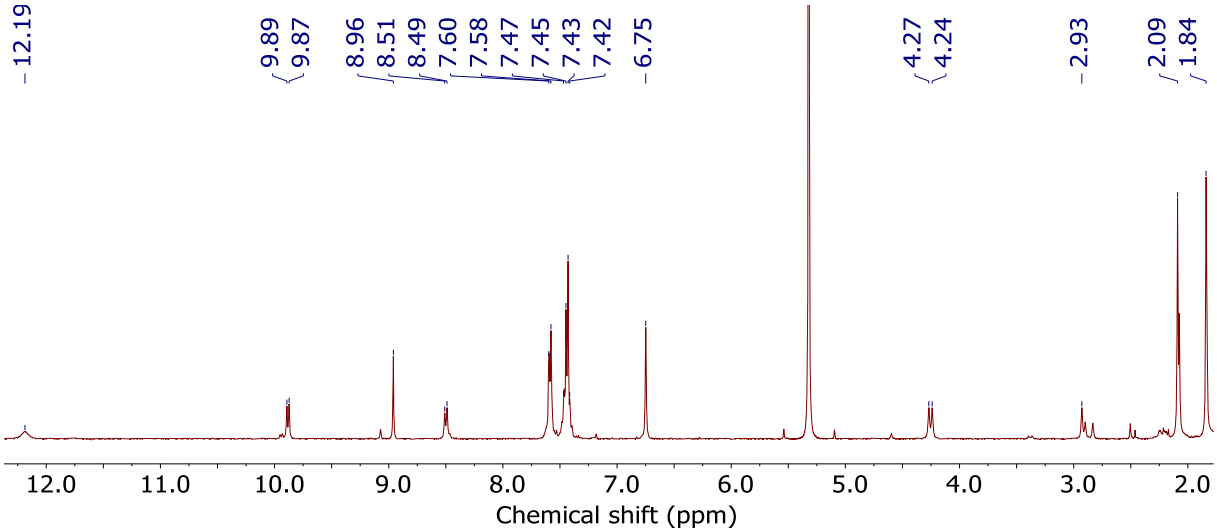

Figure S10. ^{1}H NMR spectrum of iradiated **4ooo** to PSS in CD_2Cl_2 (λ = 350 nm for 24 hours)

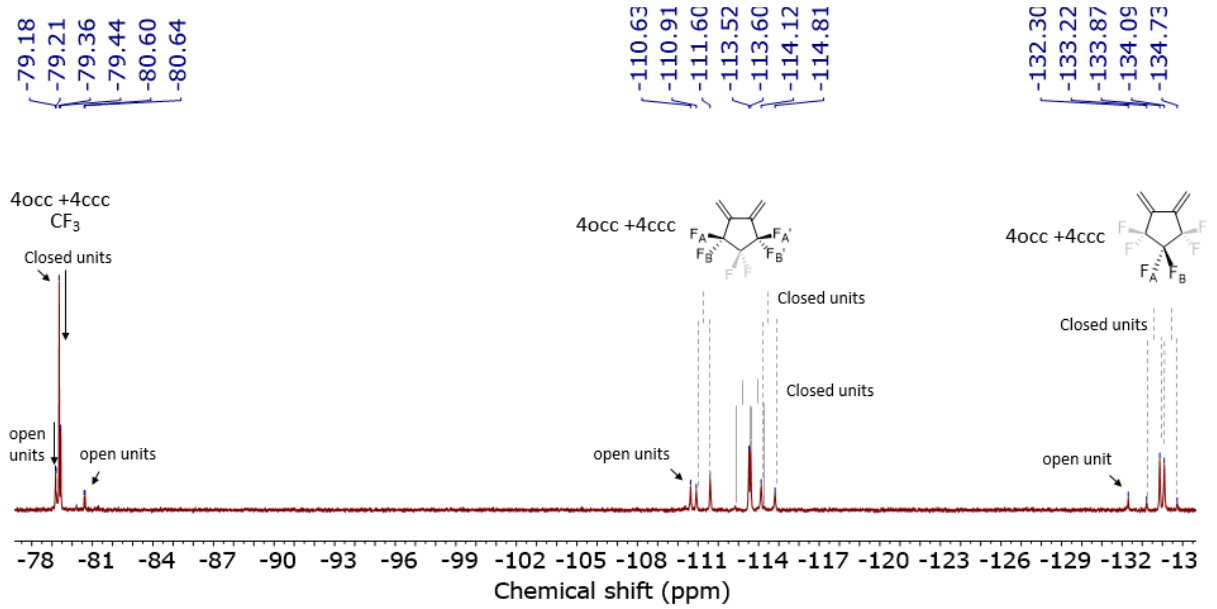

Figure S11. ^{19}F NMR spectrum of iradiated **4ooo** to PSS in CD_2Cl_2 (λ = 350 nm for 24 hours), *the pattern of the NMR spectrum is due to the presence of statistical isomers for* ***4occ*** *(occ, coc, cco)*

Compound 4ccc: ^{1}H NMR (400 MHz, CD_2Cl_2, 297K): δ 12.19 (bs, 2H, H_{phen}), 9.88 (d, 2H, ^{3}J= 8Hz, H_{phen}), 8.96 (s, 2H, H_{phen}), 8.5 (d, 2H, $^{3}J_{HH}$= *8Hz*, H_{phen}), 7.59 (d, 6H, $^{3}J_{HH}$= 8Hz, H_{ortho}), 7.44 (m, 9H, $H_{meta/para}$), 6.75 (s, 3H, H_3), 4.25 (d, 3H, H_2), 2.93 (s, 3H, H_1), 2.09 (s, 9H, CH_3), 1.84 (s, 9H, CH_3). ^{19}F NMR (376< MHz, CD_2Cl_2, 297 K): δ -79.21 (s, 6F, CF_3), -78.36 (s, 3F, CF_3), -111.25(d, 3F, $^{2}J_{FF}$= 253 Hz, external CF_2), -114.46 (d, 3F, $^{2}J_{FF}$= 253 Hz, external CF_2), -113.17 (d, 3F, $^{2}J_{FF}$= 257 Hz, external CF_2), -113.95 (d, 3F, $^{2}J_{FF}$= 257 Hz, external CF_2), -133.54 (d, 3F, $^{2}J_{FF}$= 238.5 Hz, central CF_2), -134.41 (d, 3F, $^{2}J_{FF}$= 238.5 Hz, central CF_2).

4. Thermogravimetric Analysis

Thermogravimetric Analysis were performed by using a Mettler-Toledo TGA-DSC-1 apparatus under dry nitrogen flow at a heating rate of 10 °C/min.

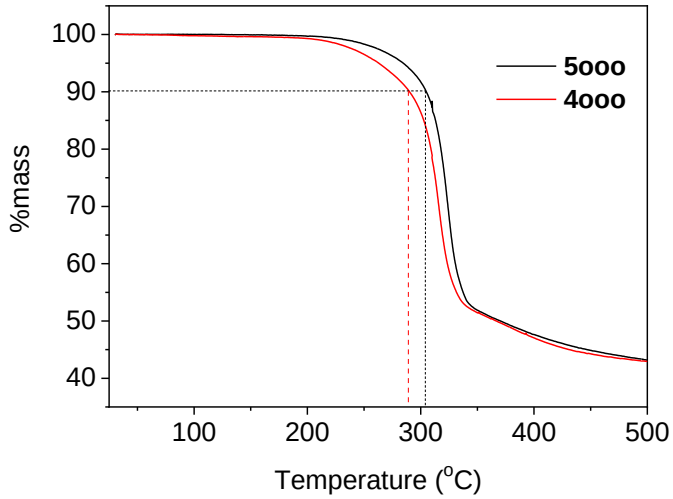

Figure S12. TGA analysis of both **4ooo** (red) and **5ooo** (black) compounds

Table S3. TGA analysis showing high T_{10D} of compounds **4ooo** and **5ooo**

	4ooo	*5ooo*
T_{10d} (°C)	303	286

5. Emission studies

For compound **4ooo**, both a with dichloromethane solution containing the compound and with PDMS doped material, the luminescence spectra were measured on a FLSP920 spectrometer (Edinburgh Instruments) at room temperature.

For compound **5ooo,** in dichloromethane solution or in PDMS doped material, the luminescence spectra were measured using a Horiba-Jobin Yvon Fluorolog-3® spectrofluorimeter, equipped with a three slit double grating excitation and emission monochromator with dispersions of 2.1 nm/mm (1200 grooves/mm). The steady-state luminescence was excited by unpolarized light from a 450 W xenon CW lamp and detected at an angle of 90° through a FGL850 filter with either a liquid nitrogen cooled solid indium/gallium/arsenic detector (850-1600 nm) or by a Symphony® II CCD detector for time resolved evolution of nIR spectrumSpectra were reference corrected for both the excitation source light intensity variation (lamp and grating) and the emission spectral response (detector and grating).

6. Fabrication of PDMS materials

The PDMS materials were prepared from the Sylgard 184 silicone elastomer kit (Dow Corning Corp., Midland, MI). A 10:1 (w/w) mixture of silicone elastomer base and silicone elastomer curing agent Sylgard 184 were used. The appropriate amounts of the two different complexes were solubilized in 1mL of dichloromethane and added to the previous mixture. Then, the reactants were thoroughly mixed in a round bottom flask for 1 hour at room temperature. The liquid mixture was sonicated for 15 minutes. Then, the solvent was removed using rotary evaporator for 10 minutes at 30 °C and under high vacuum for 30 minutes at room temperature. The viscous mixtures were transferred to crystallizing dish, aged for 24 hours at room temperature under air, and cured for 1 week at 80 °C in the oven. The elastic transparent composite materials with actual loadings (0.05% wt, 0.1% wt, 0.2% wt) and with both complexes were obtained.

References

[1] H. Al Sabea, L. Norel, O. Galangau, H. Hijazi, R. Metivier, T. Roisnel, O. Maury, C. Bucher, F. Riobe, S. Rigaut, *J. Am. Chem. Soc.* **2019**, 141, 20026.

[2] G. M. Sheldrick, *Acta Crystallogr. A Found. Adv.* **2015**, 71, 3.

[3] G. M. Sheldrick, *Acta Crystallogr. C Struct. Chem.* **2015**, 71, 3.

[4] P. van der Sluis, A. L. Spek, *Acta Crystallogr. A Found. Adv.* **1990**, 46, 194.

[5] A. Spek, *J. Appl. Crystallogr.* **2003**, 36, 7.